Research Square

Preprints are preliminary reports that have not undergone peer review.
They should not be considered conclusive, used to inform clinical practice,
or referenced by the media as validated information.

Numerical and Experimental Characterization of Melting Kinetics in Sub- Zero Thermal Energy Storage Units: Influence of Enclosure Geometry

Ankit Kumar Deshmukh
DESHANK96@GMAIL.COM
ICAR-National Dairy Research Institute
P.S. Minz
ICAR-National Dairy Research Institute
Rohit H. K
ICAR-National Dairy Research Institute
Sumit Mehta
ICAR-National Dairy Research Institute
Chitranayak Sinha
ICAR-National Dairy Research Institute

Research Article

Keywords: Phase Change Materials (PCM), Thermal Energy Storage, Heat Transfer Simulation, Python Modeling, Experimental Validation, Energy Efficiency

Posted Date: July 13th, 2026

DOI: https://doi.org/10.21203/rs.3.rs-9939079/v1

License: This work is licensed under a Creative Commons Attribution 4.0 International License.
Read Full License

Additional Declarations: No competing interests reported.

Numerical and Experimental Characterization of Melting Kinetics in Sub-Zero Thermal Energy Storage Units: Influence of Enclosure Geometry

AK Deshmukh*, PS Minz, Rohit H.K, Sumit Mehta, Chitranayak

Dairy Engineering Division, ICAR-National Dairy Research Institute, Karnal, India

Abstract

Expanding demands for thermal energy storage within cold chain logistics require container designs tailored to rapid heat transfer. Phase Change Materials (PCMs) are excellent candidates due to their high latent heat capacity, though enclosure geometry exerts critical boundary control over melting behavior. This study presents a comparative numerical evaluation tracking PCM melting kinetics across four distinct cross-sections: rectangular, square, cylindrical, and triangular.Results indicate that the rectangular cell yields the most efficient thermal response, driving the temperature from -15.0°C to 12.0°C within 50 minutes. Its high surface-area-to-volume ratio accelerates buoyancy-driven natural convection loops once past the initial phase-change band (-5°C to -2°C). Conversely, the triangular enclosure exhibited the slowest melting kinetics, terminating at a sub-zero -0.63°C due to acute vertices acting as fluid stagnant zones that choke convective movement. Statistical validation confirmed the modeling robustness, maintaining an R^2 above 0.85 across all configurations. The cornerless, symmetric boundaries of the cylindrical cell enabled the highest predictive fidelity (R^2 = 0.9826, RMSE = 0.7896°C, and MAE = 0.6100°C). These findings position rectangular geometries as optimal for high-flux energy discharge, while square and triangular shapes are suited for sustained thermal buffering.

Keywords: Phase Change Materials (PCM), Thermal Energy Storage, Heat Transfer Simulation, Python Modeling, Experimental Validation, Energy Efficiency

1. INTRODUCTION

The use of Phase Change Materials (PCMs) has advanced pointedly with the growing need for efficient Thermal Energy Storage (TES) systems. These materials are in high demand because of their considerable latent heat storage capacities, making them well-suited for applications such as moveable cold storage units and cold chain logistics systems (Izadi et al., 2025). Constancy in thermal performance have to be maintained in case to keep the product's integrity and the systems' operating efficiency.

Although thermophysical properties of PCMs have been thoroughly investigated, the effect of the container geometry on the phase change behavior is still an important consideration in system design. The geometry of the container surrounding the Phase Change Material (PCM) has been identified as a important parameter influencing the thermal charging and discharging efficiency of latent heat storage systems. Geometric construction alterations affect the thermodynamics of heat transfer by varying the surface area to provide thermal exchange and where in space the enclosure is located (Abdellatif et al., 2025). Geometries whose surface-area-to-volume ratio is larger are more likely to facilitate faster heat transfer and interaction between the PCM and ambient fluid, hence the quicker melting and solidification cycles. Those geometries which can facilitate internal natural convection of the PCM, e.g., inclined or vertical walls, also tend to induce faster and more uniform phase transition. Yet, containers with limited surface exposure or low heat transfer pathways can lead to inhomogeneous temperature gradients, hence slowing down the phase change progression. Hence, the appropriate choice of a vessel geometry for maximizing the thermal efficiency of PCM-based energy storage systems is required (Hekmat et al., 2022).

There are a number of PCM container shapes and geometries, such as cylindrical, spherical, and finned geometries. They all have been recognized to produce advantages in the aspect of enhancing thermal transfer (Karthikeyan et al., 2014; Zayed et al., 2020; Dhaidan & Khodadadi, 2015). Various PCM container geometries were calculated to evaluate their influence on thermal response when it comes to utilizing a solar dryer. It was found that rectangle geometries in the horizontal orientation exhibited the optimal melting and solidification characteristics and that cylindrical containers exhibited lesser phase change kinetics. The researchers further noted that the inclusion and configuration of fins significantly improved the rate of heat transfer for all geometries (Manikandan et al., 2024). At constant heat flow conditions, the effect of the height difference in rectangular containers for PCM on the melting behavior was studied. As the container height was raised from 12 cm to 48 cm, the time for melting increased up to 50%. This addition was attributed to greater temperature layering within the container and higher sensible heat storage in the top layers. It highlights the significance of vertical dimensioning while designing PCM containers for effective heat transfer and reduction of phase change time (Huang et al., 2010). Nevertheless this, comparative study in elementary geometries such as triangular and square containers under uniform thermal conditions is relatively less. These elementary geometries, though geometrically simple, form efficient models

for examining elementary heat transfer dynamics and their possible effect on the efficiency of thermal energy storage units in practical applications.

The containers shape influences the melting behavior of phase change materials (PCMs) in excess heat recovery of systems, as demonstrated by time-dependent 3D simulations. Recent investigations into PCM encapsulation have highlighted that while rectangular units promote high buoyancy-driven flow, cylindrical geometries provide superior radial thermal stability. Furthermore, to overcome the low thermal conductivity (k) of many PCMs, researchers have successfully integrated aluminum fins, copper nanoparticles, and metal foams to accelerate phase transitionThree different designs were tested. a standard rectangular container and two with walls that either fold inward or outward— both keeping the same cross-sectional area. The results showed that the container's shape have direct impact on degree of natural convection occurs within the molten PCM, which in turn greatly influences quickness of heat stored and moved around. Interestingly, the design with outward-folded sides at a larger angle outperformed the others, reducing the melting time by nearly a quarter, or 24.9% (Qin et al., 2022).

While the thermophysical properties of PCMs are well-documented, a research gap exists in the direct comparison of elementary container geometries—specifically triangular and square enclosures—under uniform indirect radiant-convective conditions. Most present literature focuses on enhancing heat transfer via additives or complex finned structures. This study addresses this gap by isolating the effect of geometry on melting kinetics in a standardized situation, providing a foundational model for designing portable cooling units for industry. Numerical modeling was used to analyze heat transfer through each geometry as a function of time. This research demonstrates that even subtle design decisions, such as the cell geometry can significantly influence the performance of PCM-based thermal energy storage systems. These design considerations enhance the versatility of such systems for a wide range of engineering applications.

2. Materials and methods

PCM Selection and Characterization

A 5% sodium chloride (NaCl) aqueous solution was used as the Phase Change Material (PCM) due to its specific eutectic properties and high latent heat capacity. These thermal and physical characteristics make it a primary candidate for analyzing sub-zero thermal energy storage (TES) systems, particularly for dairy cold-chain applications. The numerical model accounts for the

simultaneous effects of natural convection within the liquid phase, conductive heat transfer, and the latent heat of fusion during the transition period.

Design of Cooling Cell Geometries

This research investigates four different container geometries—rectangular, cylindrical, square, and triangular—to determine how boundary configurations influence melting front propagation and thermal discharge efficiency. The selection of these shapes reflects the most common profiles utilized in industrial energy storage and portable cooling.

To ensure a scientifically rigorous comparison, two primary design constraints were implemented:

1. Iso-Volumetric Standard: All cells were designed with a consistent internal PCM volume of 148 cm^3 to isolate the effect of shape from scale.
2. Standardized Thermal Path: The distance from the geometric centre to the inner boundary (effective radius) was maintained consistently across geometries to minimize variability in conduction-dominated heat transfer.

Dimensional Specifications

The structural dimensions were calculated to balance heat exchange efficiency with the physical requirements of phase transition:

- Rectangular Cell: Dimensions of 5.6 cm × 2.5 cm × 12 cm.
- Square Cell: Equal sides of 5.6 cm with a height of 4.7 cm to achieve the target volume.
- Triangular Cell: An equilateral profile with 9.6 cm sides and a 3.7 cm height.
- Cylindrical Cell: An inner radius (r_i) of 2.8 cm and height (h) of 6 cm.

A uniform wall thickness of 2 mm (SS-304) was maintained to facilitate rapid thermal interaction while providing structural durability. Additionally, the fabricated height of each container includes a intended headspace to accommodate the volumetric expansion of the aqueous solution during freezing, preventing mechanical stress on the welded joints.

For triangular geometry the distances from the centroid to sides and vertices, were computed in terms of inscribed radius $r = \frac{a\sqrt{3}}{6}$ and circumscribed radius $R = \frac{a\sqrt{3}}{3}$, respectively, to investigate heat transfer from different points.

Simulation approach

i. Thermal Properties

The thermal behavior of a 5% NaCl aqueous solution in different geometries was investigated using numerical simulations. The thermophysical properties used in the model include thermal conductivity k = 0.606 W/m°K, specific heat capacity cp = 3900 J/kg°K and density ρ = 1034 kg/m^3. These values were held constant throughout the simulations for all geometrical configurations.

ii. Boundary and Initial Conditions

The system was designed to simulate the melting of the PCM within containers of various geometries. The initial temperature of the solution was uniformly set to −15 °C, representing a fully frozen state. The outer stainless steel (SS-304) surfaces of the container were exposed to an air (30 °C) having convective heat transfer coefficient h = 9.0 W/m^2K. The governing boundary and initial conditions were defined as follows:

Initial condition

$$T(x, y, z, t = 0) = -15°C \quad (1)$$

Where,

T= temperature at center of PCM Cells

x,y,z= coordinates

t= time

Convective boundary condition

$$\Delta T = (T_{\text{surface}} - T_{\text{outside}}) \quad (2)$$

Where,

$T_{\text{surface}} = Temperature\ at\ surface\ of\ PCM\ cylinder$

$T_{\text{outside}} = Temperature\ maintained\ at\ hot\ air\ oven$

Symmetry condition

$$\frac{\partial T}{\partial x} = \frac{\partial T}{\partial y} = \frac{\partial T}{\partial z} = 0, at\ symmetry\ plan \quad (3)$$

Where,

x,y,z- spatial ordinates

$\frac{\partial T}{\partial x}$ – Rate of change of temperature with respect to x

Similarly, $\frac{\partial T}{\partial y}, \frac{\partial T}{\partial z}$

iii. Heat conduction

$$\rho c_p \frac{\partial T}{\partial t} = k\nabla^2 T \quad (4)$$

Where,

k	Thermal conductivity (W/m·K),
c_p	Specific heat capacity (J/kg·K)
ρ	Density of solution (kg/m³)
$\nabla^2 T$	Laplacian representing spatial temperature gradients

iv Convective heat transfer

$$-k\frac{\partial T}{\partial n} = h \cdot A\,(T_{\text{surface}} - T_{\text{outside}}) \quad (5)$$

Where,

$\frac{\partial T}{\partial n}$- Temperature gradient normal to surface

h- convective heat transfer coefficient

A- Surface area

v. Phase change

The simulation model included the influence of phase change through variation of effective heat capacity during the melting stage. This variation incorporated the latent heat of fusion L_f, reducing the rate heat rise during phase transition and speeding it up thereafter. The effective heat capacity was modeled as:

$$c_p^{\text{cff}}(T) = \begin{cases} c_p \cdot 1.5, & T < T_{\text{phase start}}, \\ c_p + \overline{L_f}, & \\ T_p \cdot 0.7, & T_{\text{phase}} - T_{\text{phase start}} \le T \le T_{\text{phase end}}, \\ c_p, & T > T_{\text{phase end}}, \end{cases} \quad (6)$$

Where,

$T_{phase\ start}$	Temperature at start of phase change
$T_{phase\ end}$	Temperature at end of phase change

C_p^{eff} Effective specific heat capacity (J/kg·K)

c_p Specific heat capacity (J/kg·K)

vi. Transient temperature

The simulation was based on the conservation of energy, accounting for both conduction and convection heat transfer mechanisms. The temperature evolution was determined using:

$$\frac{dT}{dt} = \frac{q_{conv} + q_{cond}}{m.C_p} \quad (7)$$

Where q_{conv} and q_{cond} represent the convective and conductive heat transfer rates, respectively.

vii. Energy Conservation Equation

The simulation model was controlled by the transient heat diffusion :

$$\rho c_p \frac{\partial T}{\partial t} = \frac{q_{source}}{V} + k\nabla^2 \mathrm{T} \quad (8)$$

Where,

ρ = Density of PCM (kg/m³)

C_p= Specific heat capacity at constant pressure (J/kg·K)

q_{source} -Total heat generated in volume V(W)

$k\nabla^2$- Laplacian of temperature (K/m²), representing heat diffusion in space

viii. Centre point temperature

The center-point temperature evolution was governed by:

$$\frac{dT}{dt} = \frac{q_{conv}+q_{cond}}{\rho V C_p^{eff}} \quad (9)$$

This formulation represented both heat conduction within the material and convective exchange in the boundary.

iv. Numerical implementation

The simulation model was developed using Python programming. Python software can successfully simulate latent heat storage thermal behavior using transient heat transfer equations. Programming based simulation is more flexible with input parameter settings, user-input with component dimensions, and material properties of components (Román & Hensel, 2025). The simulation domain for each geometry was discretized using a structured grid. The transient heat conduction equations were numerically integrated using the solve_ivp function from the SciPy

library. This solver is particularly suited for stiff ordinary differential equations and provides robust time integration for the heat transfer model.

Each simulation was initialized with a uniform temperature field and solved iteratively for a total duration of 50 min. Temporal and spatial discretization parameters were selected to ensure numerical stability and convergence. The simulation was conducted over a total duration of 50 min to capture the transient thermal behavior of the system. Temperature data were recorded at six specific time intervals: 0, 10, 20, 30, 40, and 50 min. These sampling points were selected to provide a detailed temporal profile of heat transfer and phase change progression throughout the simulation period. Numerical modeling using Python's solve_ivp and SciPy libraries offers high customizability for transient heat transfer. However, limitations include **increased computational intensity** for high-resolution 3D grids and **discretization challenges at acute vertices** (e.g., in the triangular cell), which contributed to a slightly higher **RMSE of 0.95°C** compared to the symmetric cylindrical cell.

To ensure consistency and comparability across different enclosure geometries, the grid resolution was carefully adjusted for each configuration. This adjustment was made to maintain an equivalent volume for all geometries and to achieve a representative spatial resolution that accurately captures thermal gradients and phase boundaries. The tailored grid resolutions helped preserve numerical stability and improve the accuracy of simulation results.

vi. Visualization and Analysis

Spatial temperature profiles were visualized using 3D scatter plots and heatmaps. These visualizations enabled the tracking of temperature progression from the outer surface to the core. For comparative analysis, the center temperature of each geometry was extracted over time to assess the relative melting dynamics.

Experimental setup

The experiment was conducted using custom-designed containers shaped into square and triangular profiles. These geometries were fabricated from stainless steel sheets, cut and welded based on calculated dimensions to ensure equal internal volumes across shapes. All joints were sealed to prevent leakage. The fabricated test rig illustrated in Figure 2, which shows the top and side views of the experimental setup. A 5% sodium chloride solution was prepared using distilled water, mixed thoroughly to achieve uniform salinity. Each container was filled with an

identical volume of this solution and kept in a deep freezer until the internal temperature of the solution reached −15 °C, ensuring complete solidification under controlled conditions (Siva et al., 2010). To monitor the thermal response during the melting phase, platinum resistance temperature sensors (PT-100) were inserted at the center of each container to capture the core temperature. More sensors were installed on the inner walls to monitor any variation of heat absorption in space. These sensors were interfaced with a data scanning logger, which monitored temperature continuously at regular time intervals for precise profiling (Mancin et al., 2022).

After freezing, the containers were straightaway subjected inside a hot air oven at 30 °C for simulating uniform ambient heating conditions. This temperature was chosen to imitate a controlled convective environment common in laboratory-scale melting tests. The computational and experimental techniques used are explained in detail in the flowchart 1 shown. It was the purpose to observe the process of melting and record the thermal response specific to every geometry.

Validation using experimental results

Experimental observations of center-point temperatures were measured by PT-100 sensors placed in PCM cells. These values were directly compared with simulation results at matching time steps (0 to 50 min). Figure 3 shows the experimental setup used to observe the temperature profile of solution melting in containers of different geometries. Simulation results were plotted against the experimental data to assess the model's predictive accuracy. To estimate the accuracy of the model, the simulation center temperatures were compared with experimental data at 0, 10, 20, 30, 40, and 50 min time intervals. The root-mean-square error (RMSE) was determined and was low, showing close agreement between the two sets of data. The minimal deviation verifies the ability of the simulation to represent the real thermal behavior during the melting process

Simulation Outputs

The model produced time-dependent center-point temperatures as well as visualized spatial thermal gradients in each container geometry.The outputs allowed for a complete comparison of heat transfer efficiency as well as melting dynamics, providing insight into the impact of container geometry on thermal behavior.

Result and Discussion

Phase Change Dynamics and Natural Convection

The transition from conduction to natural convection was observed as the PCM temperature surpassed the -5°C to -2°C range. In the rectangular cell, planar walls facilitated intense buoyancy-driven currents, causing the melting front to propagate faster than in the cylindrical rig. This is evidenced by the simulation's ability to track the 3D temperature gradient toward the core, as visualized in Figures 5–8.

Thermal response analysis

The thermal simulations highlighted clear distinctions in melting behaviour among the four container geometries. Rectangular geometry demonstrated the fastest thermal response, with the temperature rising from −15.0 °C to 12.0 °C in just 50 min. Notable temperature milestones included −8.58 °C at 10 min and 4.43 °C at 40 min. This accelerated heating can be credited to its high surface-to-volume ratio, which enhanced both conductive and convective heat transfer. The uniform structure of the rectangular cell allowed for an even temperature distribution, and the melting process displayed two distinct phases: an initial conduction-dominated regime, followed by the onset of natural convection, particularly after the latent heat phase-change interval between −5.0 °C and −2.0 °C (Fig. 5). As melting progressed, the initially symmetric front evolved into an asymmetric one due to convective currents (Huo et al., 2021; Parsazadeh & Duan, 2018).

The cylindrical cell also exhibited efficient thermal behavior but at a more moderate rate, with the temperature reaching 3.97 °C at 50 min. It showed a consistent increase from −10.73 °C at 10 min to −3.47 °C at 40 min (Fig. 6). Its radial symmetry contributed to concentric temperature gradients, with heat propagating inward from the curved surface. This structure supports balanced energy distribution and minimizes thermal hotspots. The cylindrical design’s smooth phase-change transition and stable temperature profile make it favorable for systems requiring uniform thermal performance and moderate response time (Yan et al., 2022).

In contrast, the triangular enclosure recorded the slowest temperature rise, ending at only −0.63 °C after 50 min. Starting from −15.0 °C, the PCM reached −10.45 °C at 10 min and −5.05 °C at 40 min. The angular configuration contributed to uneven heat transfer, with shorter conduction paths along edges enabling quicker melting in those areas, while the center remained relatively cold (Fig. 7). Limited fluid circulation and geometric constraints hindered the

development of natural convection, slowing the phase-change process (Soodmand et al., 2022). These characteristics, although reducing the melting rate, enhanced cooling retention, which is advantageous for thermal buffering applications. Consequently, the phase-change process was delayed (Fig. 8). This behavior suggests that triangular PCM cells are better suited for applications that demand thermal stability and gradual energy release.

The superior performance of the rectangular geometry is fundamentally linked to its planar surfaces, which allow for the unhindered development of buoyancy-driven circulation cells. As the melting front propagates from the walls toward the core (visualized in Figure 5), the liquid PCM experiences a lower flow resistance compared to the **triangular geometry**, where acute corners act as stagnant zones that hinder convective heat transfer and lead to slower phase-change kinetics. For related research, triangular and cylindrical cells had higher melting durations of about 5000 seconds and 4250 seconds, respectively, attributed to restricted surface exposure and inefficiencies in localized conduction (Soodmand et al., 2022). The findings highlight the significant role played by container shape in PCM performance, with cylindrical and square geometries tending to experience delayed melting because of diminished buoyancy effects and the delayed development of convective flow (Mishra et al., 2022)

Temperature variations with time

A close comparison of temperature profiles for rectangular, cylindrical, square, and triangular test rigs reveals the different thermal behavior in these test rig geometries. The rectangular test rig was always found to have better cooling efficiency due to the quickest rise in temperature among all time intervals. Starting from an initial temperature of −15.6 °C, the rectangular cell reached 0 °C within 40 minutes and subsequently attained 13 °C at t = 50 min. This is because the rectangular shape has a greater surface-area-to-volume ratio, which increases the efficiency of heat dissipation through maximal exposure to external convection. The rectangular geometry outperformed others throughout the experiment, reaching **0°C within 40 minutes**. This is attributed to its high surface-area-to-volume ratio, which promotes earlier onset of natural convection. Conversely, the triangular cell exhibited the slowest rise, reaching only **-0.63°C after 50 minutes**, due to localized thermal resistance at its vertices. Comparable findings has been documented in an experiment examining the effects of varying inclinations of rectangular phase change material (PCM) containers on melting kinetics, melting efficiency improvement was largely due to the enhanced natural convection currents within the PCM

(Abdulmunem et al. 2020). Compared to that, moderate performance was indicated by the cylindrical rig. From a starting temperature of -15 °C, it rose to -4.4 °C at t=40 min and 4.3 °C at t =50 min showing a reduced thermal response compared to the rectangular rig. The reason for this is the cylindrical geometry having a curved surface, which helps in even heat distribution and minimization of localized thermal gradients (Cheng & Chang, 2003).

However, the limited effectiveness of buoyancy-driven convection in the cylindrical enclosure results in lower overall heat transfer efficiency. These results was in agreement with past research, such as, that of Jones et al., which show that the low convective flow patterns and heat transfer limitations of the cylindrical PCM container cause it to melt at a reduced rate than the rectangular configuration. Unlike the rectangular configuration that promotes natural convection and maximizes the melting rate, the cylindrical enclosure curvature inhibits strong buoyancy-driven convective flows (Jones et al., 2006).

The square rig's thermal response was slower, starting at -15.0 °C and cresting at 0.1 °C at t=50min. Due to the symmetrical shape, a square cavity inhibits the formation of strongest natural convection currents, hence slowing down the process of melting. The trapping of heat at localized regions with limited circulation brings about temperature gradients, reducing heat transmission efficiency (Younis et al., 2024). All the same, triangular rig performance was mid-range, starting at -15.0°C and descending as low as -0.6°C by t= 50min. The geometries have smaller surface-area-to-volume ratios than the rectangular rig, and they therefore are heat exchange efficiency-limited and cool more slowly. As shown in Figure 9, temperature profiles for all geometries distinguish by clearly showing the superior thermal performance of the rectangular shape, which is ahead of the others in all time periods. In addition, Table 4 gives a detailed report of the temperature variations for all geometries and shows the effectiveness of the rectangular rig at all stages of the experiment. For example, at t =20 min, the rectangular rig was -4.9 °C, whereas the square, triangular, and cylindrical rigs were -8.4 °C, -5.7 °C, and -8.0 °C, respectively. Such results are representative of the contribution of geometry to heat dissipation, in which the rectangular geometry is exposed to maximum cooling efficiency as a result of its optimal surface area-to-volume ratio.

Simulated and experimental temperature profiles

The correctness of the computational model was measured by comparing its center-point temperature predictions with corresponding experimental data for all four PCM container

geometries over the specified time period (Fig. 10). Among the geometries tested —rectangular, square, triangular, and cylindrical—the cylindrical vessel had the best fit with the empirical data, having an R^2 value of 0.9826. The absence of corners or abrupt geometric transitions facilitates smoother thermal gradients, enabling the model to closely replicate the experimental thermal response (Nussbaum et al., 2022; Verma & Barman, 2025).

The R^2 of 0.9508 for rectangular test rig was slightly lower as compared to cylinder, but still robust as a model. This may be because the elongated shape naturally conducts heat along its longer axis, a tendency fostered by its uniform wall thickness and flat ends as explained by Liu et al, these characteristics allow for a consistent temperature profile throughout melting—an effect well-represented in the numerical simulation(Liu et al., 2022).

For the square-shaped container, an R^2 of 0.951 was achieved, showing again a very high fidelity between similarly high fidelity between the simulation and experimental data.. The symmetry and equal dimensions of the square geometry allowed for balanced thermal propagation, minimizing complexity in heat transfer pathways. This enabled the numerical model to reproduce the observed temperature evolution with commendable accuracy(Łach & Svyetlichnyy, 2025).

In contrast, the triangular container exhibited the lowest R^2 value, at 0.926. Although this still indicates a good level of agreement, the comparatively lower value suggests greater challenges in accurately modeling the thermal behavior of this geometry. The presence of acute angles and non-uniform cross-sections introduces localized thermal resistances and non-linear heat flow, particularly at the vertices. These features are inherently more difficult to capture in a discretized computational domain and may lead to slight deviations between simulation and reality(Olabode Thomas Olakoyejo, 2012). Despite these shape-specific differences, the numerical model successfully reproduced the key temperature evolution trends across all geometries. As shown in Figure 9, the R^2 values collectively affirm the model's robustness and its capability to accurately simulate conduction-dominated phase change behavior. Minor discrepancies observed can be attributed to necessary simplifications in boundary conditions, assumptions of material homogeneity, or uncertainties associated with experimental measurements.

Evaluation of simulation accuracy for different container geometries

To rigorously assess the predictive fidelity of the simulation model, Figure 10 presents a

comprehensive three-part evaluation involving center temperature profiles, error distribution, and quantitative performance metrics across cylindrical, rectangular, square, and triangular container geometries under melting conditions.

Phase Change Dynamics Comparison

The top-left plot in Figure 11 illustrates the time-resolved temperature evolution at the geometric center of each container, comparing experimental data (dashed lines) with simulated predictions (solid lines) over a 50-minute melting cycle. Notably, the phase change zone (spanning approximately 0°C to 5°C, highlighted in gray) serves as a critical interval for model validation. Among all configurations, the cylindrical container demonstrates the closest agreement, with a near-complete overlap of simulation and experimental curves throughout the entire melting duration. The average deviation within the phase transition window for the cylindrical case remains within ±0.3°C, underscoring the model's robustness in predicting the latent heat absorption and temperature stabilization characteristics.

The rectangular container also exhibits high agreement, with slight deviations (~±0.5°C) primarily after 30 min when melting nears completion. In contrast, the square and triangular geometries show noticeable divergence, especially beyond the 35-minute mark. These deviations suggest limitations in heat distribution modeling near corners or abrupt geometric discontinuities, which lead to localized under- or over-predictions of thermal response.

Model Performance Metrics

A rigorous statistical assessment was executed across all four container shapes to verify the precision of the numerical model against empirical data. The primary performance indicators—the Coefficient of Determination (R^2), Root Mean Square Error (RMSE), Mean Absolute Error (MAE), and Bias—are detailed in Table 5. Out of every configuration evaluated, the cylindrical cell demonstrated the highest predictive accuracy. This geometry achieved an R^2 of 0.9826 while minimizing global error margins (RMSE = 0.7896°C and MAE = 0.61°C). The recorded negative Bias of -0.50°C indicates that the simulation maintained a minor, systematic overestimation of the actual experimental temperatures. This high-tier predictive precision stems directly from the cylinder's perfect geometric symmetry and cornerless boundary profile, which establish steady, uniform heat dispersion pathways (Barakat & Sun, 2024).

The rectangular enclosure followed closely in terms of tracking macro-level directional trends,

yielding an R^2 of 0.9508 and a comparable negative Bias of -0.4850°C. Even so, the corresponding RMSE spiked noticeably to 1.9489°C. Because the RMSE metric disproportionately penalizes larger individual deviations, this sharp divergence from the lower MAE (1.3317°C) reveals that the simulation and experimental curves drifted apart aggressively during the final stages of the melting cycle.

On the other end of the spectrum, the square and triangular configurations caused a distinct drop-off in model reliability, resulting in lower R^2 values of 0.8845 and 0.8523, respectively. The square geometry generated an RMSE of 1.6007°C paired with a positive Bias of +0.9217°C. Meanwhile, the triangular setup proved to be the most problematic profile in the study, logging a steep MAE of 1.4300°C and an equally high positive Bias of +1.4300°C.

In contrast to the cylindrical and rectangular trends, these positive bias scores prove that the simulation consistently underestimated physical temperatures within the square and triangular cells. This shift highlights a well-documented bottleneck in computational thermal dynamics, tracking moving phase-change fronts through sharp, acute vertices is incredibly complex, particularly where restricted fluid loops create highly anisotropic heat flows (Soodmand et al., 2023).

Ultimately, this verification routine demonstrates that while jagged boundary profiles present major mathematical challenges, the underlying numerical framework remains highly capable on a macro-level, keeping R^2 correlations safely above the 0.85 threshold across all evaluated configurations.

Conclusion

This research highlights how the physical shape of a container fundamentally dictates the melting pathways and thermal behavior of Phase Change Materials (PCMs). By coupling experimental runs with numerical models across four distinct cross-sections—cylindrical, rectangular, square, and triangular—we mapped out how geometry alters latent heat storage performance.

Our core findings indicate that:

- **Geometry Governs Charging Rates:** Container geometry acts as the primary bottleneck or catalyst for heat transfer. The rectangular cell outpaced all other designs, driving the PCM temperature from -15.0°C up to 12.0°C within a 50-minute window. This rapid thermal response stems directly from its high surface-area-to-volume ratio and flat boundary walls. These features accelerate the onset of strong, buoyancy-driven natural

convection loops once the material clears its initial phase-change band (-5°C to -2°C).

- **Vertices Restrict Fluid Mechanics:** While the rectangular domain reached 0°C by the 40-minute mark, the triangular cell lagged severely, finishing the 50-minute test at a sub-zero -0.63°C. This performance drop proves that sharp, acute corners function as fluid dead zones. These restrictive vertices physically choke convective plumes, stall boundary-layer fluid movement, and build up localized thermal resistance that slows down overall melting kinetics.
- **Quantifying Simulation Limits:** The mathematical model successfully tracked macro-level melting trends across every geometry, maintaining a solid correlation ($R^2 > 0.85$). It proved exceptionally stable when handling the corner-less, symmetric bounds of the cylindrical cell ($R^2 = 0.9826$, RMSE = 0.7896°C, MAE = 0.6100°C), making it ideal for conduction-heavy, uniform setups. However, sharp-cornered boundaries forced the model to systematically underestimate reality. This is clear from the heavy positive biases recorded in the square (+0.9217°C) and triangular (+1.4300°C) tests, pointing to areas where standard phase-change algorithms struggle with anisotropic flow.
- **Design Rules for Thermal Units:** These outcomes offer practical guidelines for tailoring latent heat storage units to specific engineering needs. Rectangular shapes are best suited for high-flux setups needing rapid energy dump or capture rates, such as quick-chilling milk storage facilities. Conversely, triangular and square configurations offer a natural buffer, making them highly effective for systems that require a slow, controlled, and sustained release of latent heat over extended periods.

In summary, this work provides a verified, highly accurate modeling approach capable of predicting complex phase-change behavior under varying physical constraints. The empirical data and specific error profiles established here provide a solid foundation for industrial design teams to optimize container shapes based on targeted thermal loads.

Funding

This research was supported by institutional funding from the ICAR-National Dairy Research Institute (NDRI), Karnal, India. The author also gratefully acknowledges financial assistance received in the form of a Junior Research Fellowship (JRF) and Senior Research Fellowship (SRF) from the University Grants Commission (UGC), Government of India.

References

Abdellatif, H. E., Belaadi, A., Arshad, A., Chai, B. X., Alshaikh, I. M. H., & Ghernaout, D. (2025). Advancing thermal energy storage: Unravelling the optimal orientation of annular phase change material containers within the tank. *Case Studies in Thermal Engineering*, *68*, 105931. https://doi.org/10.1016/j.csite.2025.105931

Barakat, A., & Sun, B. (2024). Enhanced convective heat transfer in new triply periodic minimal surface structures: Numerical and experimental investigation. *International Journal of Heat and Mass Transfer*, *227*, 125538. https://doi.org/10.1016/j.ijheatmasstransfer.2024.125538

Cheng, C.-H., & Chang, M.-H. (2003). Shape design for a cylinder with uniform temperature distribution on the outer surface by inverse heat transfer method. *International Journal of Heat and Mass Transfer*, *46*(1), 101–111. https://doi.org/10.1016/S0017-9310(02)00226-0

Dhaidan, N. S., & Khodadadi, J. M. (2015). Melting and convection of phase change materials in different shape containers: A review. *Renewable and Sustainable Energy Reviews*, *43*, 449–477. https://doi.org/10.1016/j.rser.2014.11.017

Hekmat, M. H., Haghani, M. H. K., Izadpanah, E., & Sadeghi, H. (2022). The influence of energy storage container geometry on the melting and solidification of PCM. *International Communications in Heat and Mass Transfer*, *137*, 106237. https://doi.org/10.1016/j.icheatmasstransfer.2022.106237

Huang, L., Noeres, P., Petermann, M., & Doetsch, C. (2010). Experimental study on heat capacity of paraffin/water phase change emulsion. *Energy Conversion and Management*, *51*(6), 1264–1269. https://doi.org/10.1016/j.enconman.2009.12.038

Huo, Y., Pang, X., & Rao, Z. (2021). Heat transfer enhancement in thermal energy storage using phase change material by optimal arrangement. *International Journal of Thermal Sciences*, *161*, 106736. https://doi.org/10.1016/j.ijthermalsci.2020.106736

Izadi, M., Pop, I., Shehzad, S. A., Alqurashi, F., Mohamed, M. H., Hajjar, A., & Mahariq, I. (2025). Comprehensive review of optimization strategies for phase change materials: Techniques, applications, and challenges in thermal storage systems. *International Communications in Heat and Mass Transfer*, *166*, 109123. https://doi.org/10.1016/j.icheatmasstransfer.2025.109123

Jones, B. J., Sun, D., Krishnan, S., & Garimella, S. V. (2006). Experimental and numerical study of melting in a cylinder. *International Journal of Heat and Mass Transfer*, *49*(15–16), 2724–2738. https://doi.org/10.1016/j.ijheatmasstransfer.2006.01.006

Karthikeyan, S., Ravikumar Solomon, G., Kumaresan, V., & Velraj, R. (2014). Parametric studies on packed bed storage unit filled with PCM encapsulated spherical containers for low temperature solar air heating applications. *Energy Conversion and Management*, *78*, 74–80. https://doi.org/10.1016/j.enconman.2013.10.042

Łach, Ł., & Svyetlichnyy, D. (2025). Advances in Numerical Modeling for Heat Transfer and Thermal Management: A Review of Computational Approaches and Environmental Impacts. *Energies*, *18*(5), 1302. https://doi.org/10.3390/en18051302

Liu, D., Xie, K., Zhang, H., Qiang, Y., Yang, D., Wang, Z., Zhu, L., Akkurt, N., Du, Y., Shen, M., Zhong, L., Yu, F., & Xu, Q. (2022). Numerical evaluation of convective heat transfer properties of two-dimensional rotating PCM melt in the unilaterally heated rectangular container. *Renewable Energy*, *193*, 920–940. https://doi.org/10.1016/j.renene.2022.05.009

Manikandan, S., Muthuvairavan, G., Samykano, M., & Natarajan, S. K. (2024). Numerical

simulation of various PCM container configurations for solar dryer application. *Journal of Energy Storage*, *86*, 111294. https://doi.org/10.1016/j.est.2024.111294

Mishra, G., Memon, A., Gupta, A. K., & Nirmalkar, N. (2022). Computational study on effect of enclosure shapes on melting characteristics of phase change material around a heated cylinder. *Case Studies in Thermal Engineering*, *34*, 102032. https://doi.org/10.1016/j.csite.2022.102032

Nussbaum, J., Dietrich, B. E., Wilm, B. J., & Pruessmann, K. P. (2022). Thermal variation in gradient response: Measurement and modeling. *Magnetic Resonance in Medicine*, *87*(5), 2224–2238. https://doi.org/10.1002/mrm.29123

Olabode Thomas Olakoyejo. (2012). *Geometric Optimisation of Conjugate Heat Transfer in Cooling Channels with Different Cross-sectional Shapes* [University of Pretoria]. https://repository.up.ac.za/items/6b12448d-e735-43ef-b277-34efc2f57df5

Parsazadeh, M., & Duan, X. (2018). Numerical study on the effects of fins and nanoparticles in a shell and tube phase change thermal energy storage unit. *Applied Energy*, *216*, 142–156. https://doi.org/10.1016/j.apenergy.2018.02.052

Qin, Z., Ji, C., Low, Z. H., Tong, W., Wu, C., & Duan, F. (2022). Geometry effect of phase change material container on waste heat recovery enhancement. *Applied Energy*, *327*, 120108. https://doi.org/10.1016/j.apenergy.2022.120108

Román, F., & Hensel, O. (2025). Latent-dry: Solar drying with latent heat storage in Python, Fortran and TRNSYS. *SoftwareX*, *29*, 101999. https://doi.org/10.1016/j.softx.2024.101999

Siva, K., Lawrence, M. X., Kumaresh, G. R., Rajagopalan, P., & Santhanam, H. (2010). Experimental and numerical investigation of phase change materials with finned encapsulation for energy-efficient buildings. *Journal of Building Performance*

Simulation, *3*(4), 245–254. https://doi.org/10.1080/19401491003624224

Soodmand, A. M., Azimi, B., Nejatbakhsh, S., Pourpasha, H., Farshchi, M. E., Aghdasinia, H., Mohammadpourfard, M., & Zeinali Heris, S. (2023). A comprehensive review of computational fluid dynamics simulation studies in phase change materials: Applications, materials, and geometries. *Journal of Thermal Analysis and Calorimetry*, *148*(20), 10595–10644. https://doi.org/10.1007/s10973-023-12438-0

Soodmand, A. M., Nejatbakhsh, S., Pourpasha, H., Aghdasinia, H., & Heris, S. Z. (2022). Simulation of melting and solidification process of polyethylene glycol 1500 as a PCM in rectangular, triangular, and cylindrical enclosures. *Alexandria Engineering Journal*, *61*(11), 8431–8456. https://doi.org/10.1016/j.aej.2022.02.011

Verma, G., & Barman, R. N. (2025). Optimized heat transfer and drag reduction through corner modifications in square cylinders immersed in power-law fluids. *Physics of Fluids*, *37*(2), 023110. https://doi.org/10.1063/5.0252830

Yan, Z., Yang, T., Li, S., Yang, Z., Yu, Z. (Jerry), & Zhang, G. (2022). Unconstrained melting of phase change material in cylindrical containers inside hot water tanks: Numerical investigation and effect of aspect ratios. *Journal of Energy Storage*, *47*, 103647. https://doi.org/10.1016/j.est.2021.103647

Younis, O., Mozaffari, M., Ahmed, A., & Ghalambaz, M. (2024). Improvement of Latent Heat Thermal Energy Storage Rate for Domestic Solar Water Heater Systems Using Anisotropic Layers of Metal Foam. *Buildings*, *14*(8), 2322. https://doi.org/10.3390/buildings14082322

Zayed, M. E., Zhao, J., Li, W., Elsheikh, A. H., Elbanna, A. M., Jing, L., & Geweda, A. E. (2020). Recent progress in phase change materials storage containers: Geometries, design considerations and heat transfer improvement methods. *Journal of Energy Storage*, *30*,

101341. https://doi.org/10.1016/j.est.2020.101341

Tables

Nomenclature

ρ	Density of solution (kg/m³)
K	Kelvin
c_p	Specific heat capacity (J/kg·K)
k	Thermal conductivity (W/m·K),
T	Temperature (K)
t	Time (s)
A_s	Surface area (m^2)
$T_{phase\ start}$	Temperature at start of phase change
$T_{phase\ end}$	Temperature at end of phase change
C_p^{eff}	Effective specific heat capacity (J/kg·K)
$℃$	Degree centigrade
$\nabla^2 T$	Laplacian representing spatial temperature gradients,
q_{source}	Heat generated or absorbed (e.g., latent heat during phase change),
q_{conv}	Heat transfer due to conduction
q_{cond}	Heat transfer due to convection
V	Control volume
L_f	Latent heat of fusion
h_{conv}	Convective heat transfer coefficient (W/m^2k)
c_p	Specific heat capacity (J/kg·K)

Table 1: Geometry specification

Geometry	Dimensions for 148 cm^3 PCM	Total Internal Volume (incl. Expansion Gap)
Rectangular	5.6 cm (a) × 2.5 cm (b) × 10.6 cm (l)	~160 cm^3
Cylindrical	r_i = 2.8 cm,, h = 6.0 cm	~160 cm^3
Square	5.6 cm (a) × 5.6 cm (a) × 4.7 cm (l)	~160 cm^3
Triangular	Side (a) = 9.6 cm, Length (l) = 3.6 cm	~160 cm^3
Legs support for each cell having height	20 mm	

Table 2: Thermal Properties of 5% NaCl Solution

Properties	Values
Thermal conductivity (k)	0.606 W/m·K
Density (ρ)	1034 kg/m³
Specific heat capacity (c_p)	3900 J/kg·K
Latent heat of fusion (L_f)	334000 J/kg
Phase change start temperature (T_phase_start)	-5 °C
Phase change end temperature (T_phase_end)	-2 °C

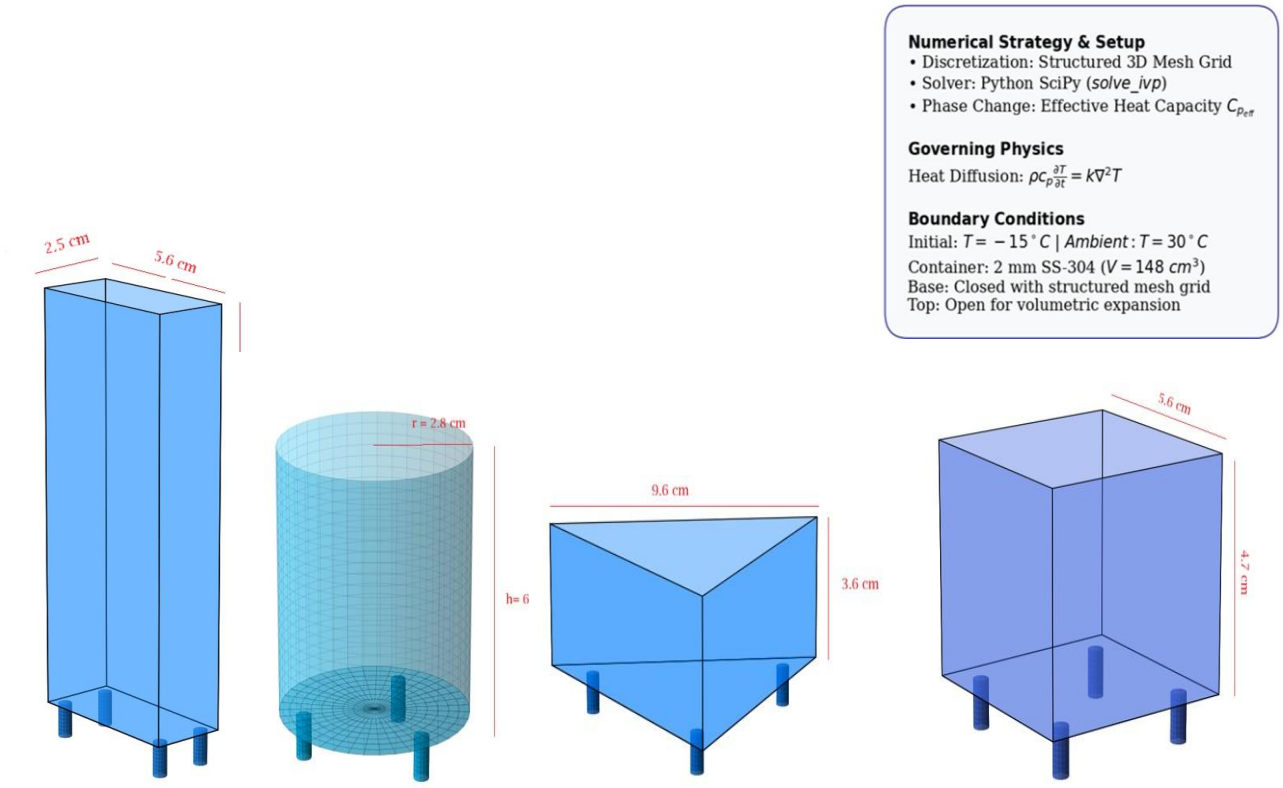
Table 3: Simulation parameters

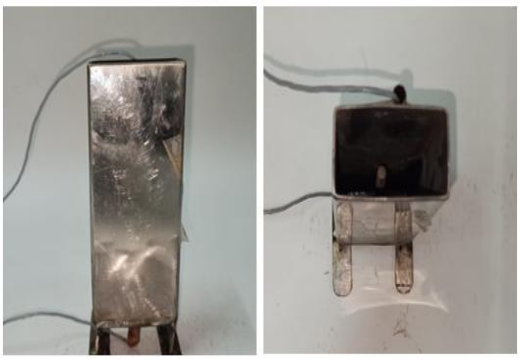
Constants	value
Initial temperature (T_initial)	-15 °C
External temperature (T_outside)	30 °C
Time steps	10 min intervals
Total simulation time	50 min
Base convective heat transfer coefficient (h_base)	9 W/m²·K
Dynamic heat transfer function	Varies with T

Table 5: Performance Metrics:

Geometry	R^2	RMSE	MAE	Bias
Rectangular	0.9508	1.9489	1.3317	-0.4850
Square	0.8845	1.6007	1.2417	0.9217
Triangular	0.8523	1.8840	1.4300	1.4300
Cylindrical	0.9826	0.7896	0.6100	-0.5000

Figure: 1 Schematic diagram of designed geometry





a) Rectangular cell



b) Cylindrical cell



c) Triangular cell



d) Square cell

Figure: 2 PCM cell container

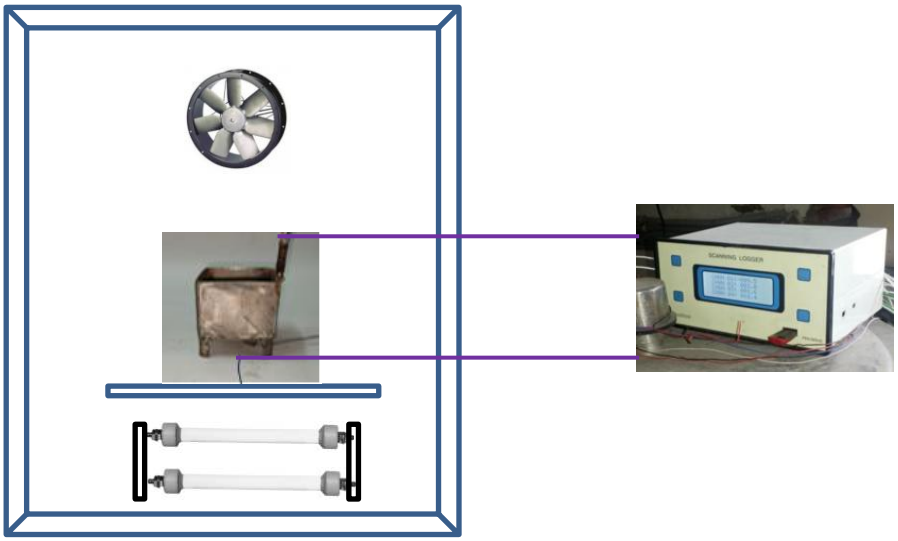


Figure: 3 Experimental setup based on in-direct radiative convective environment

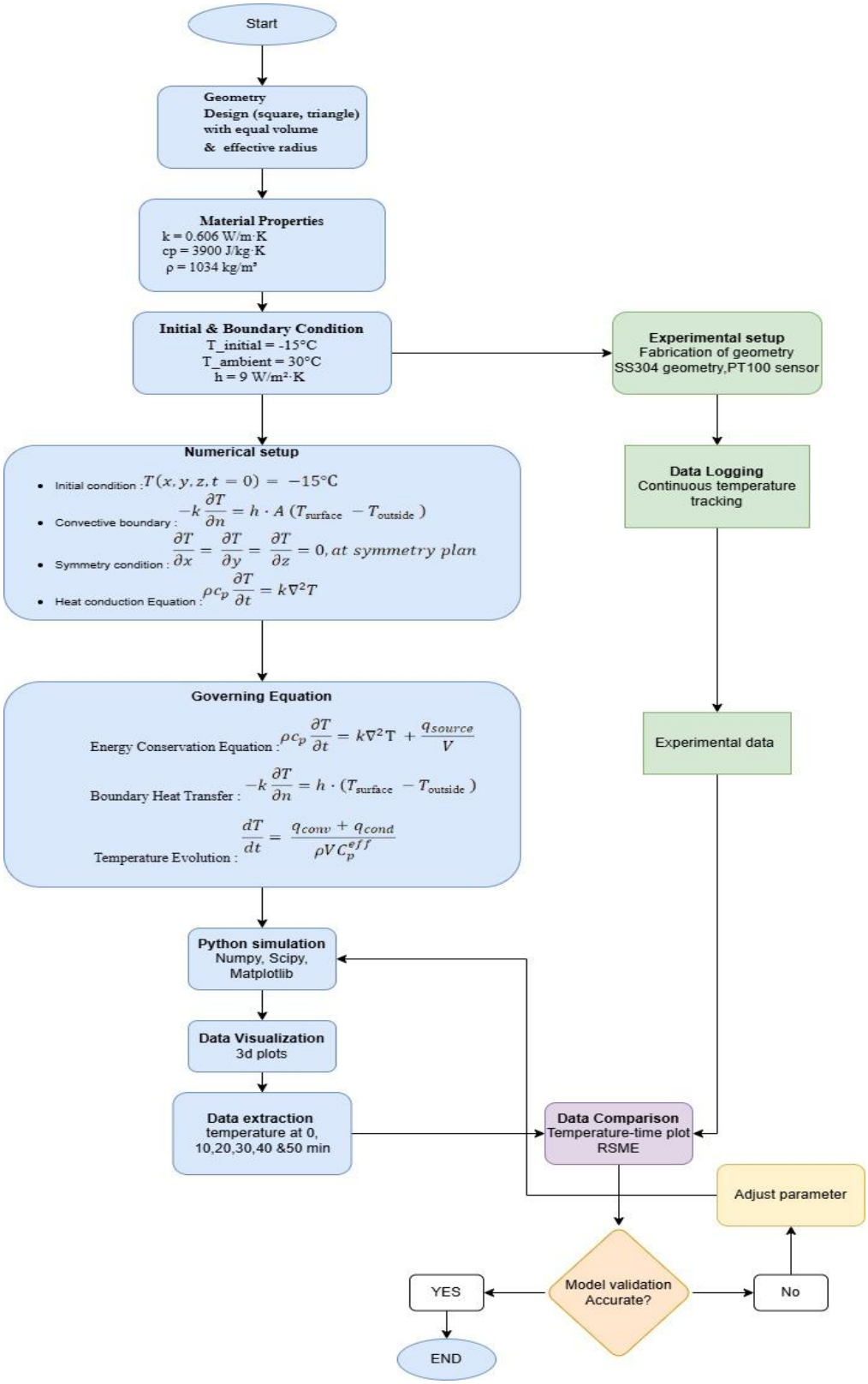
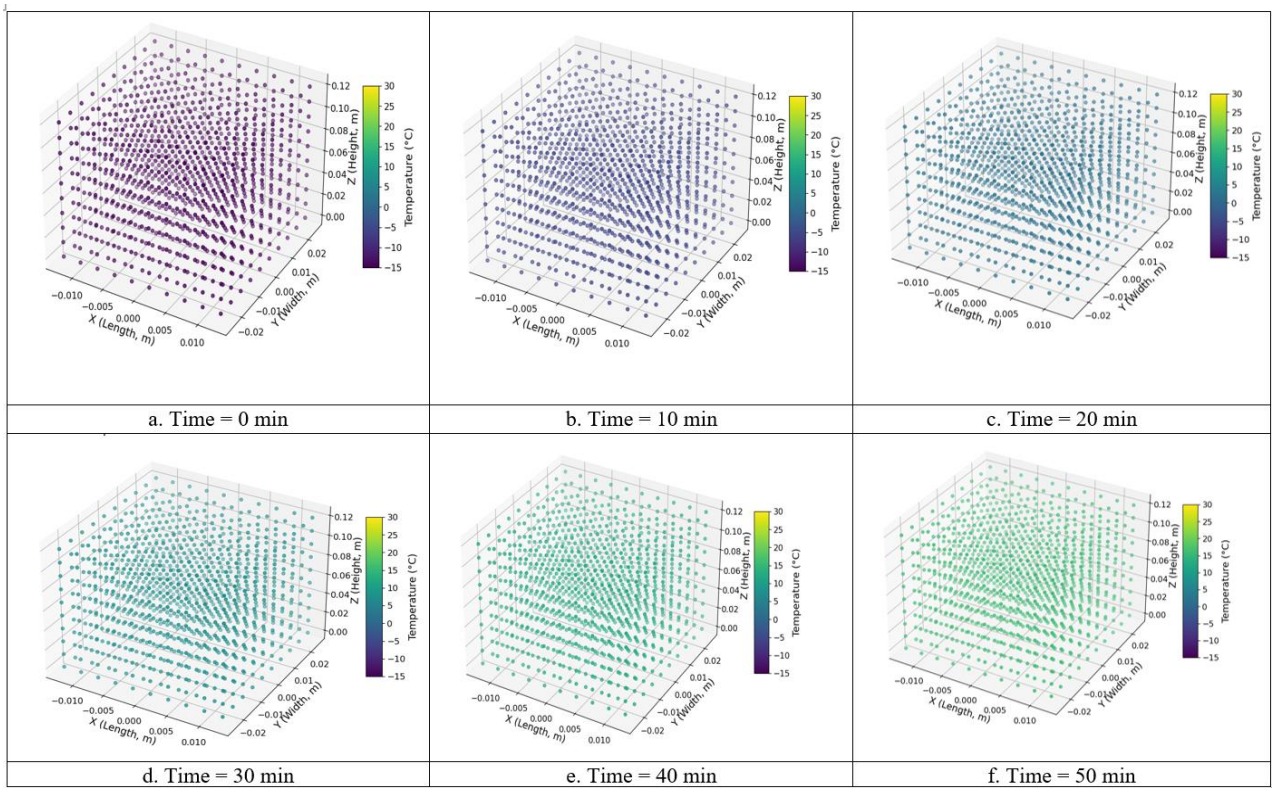
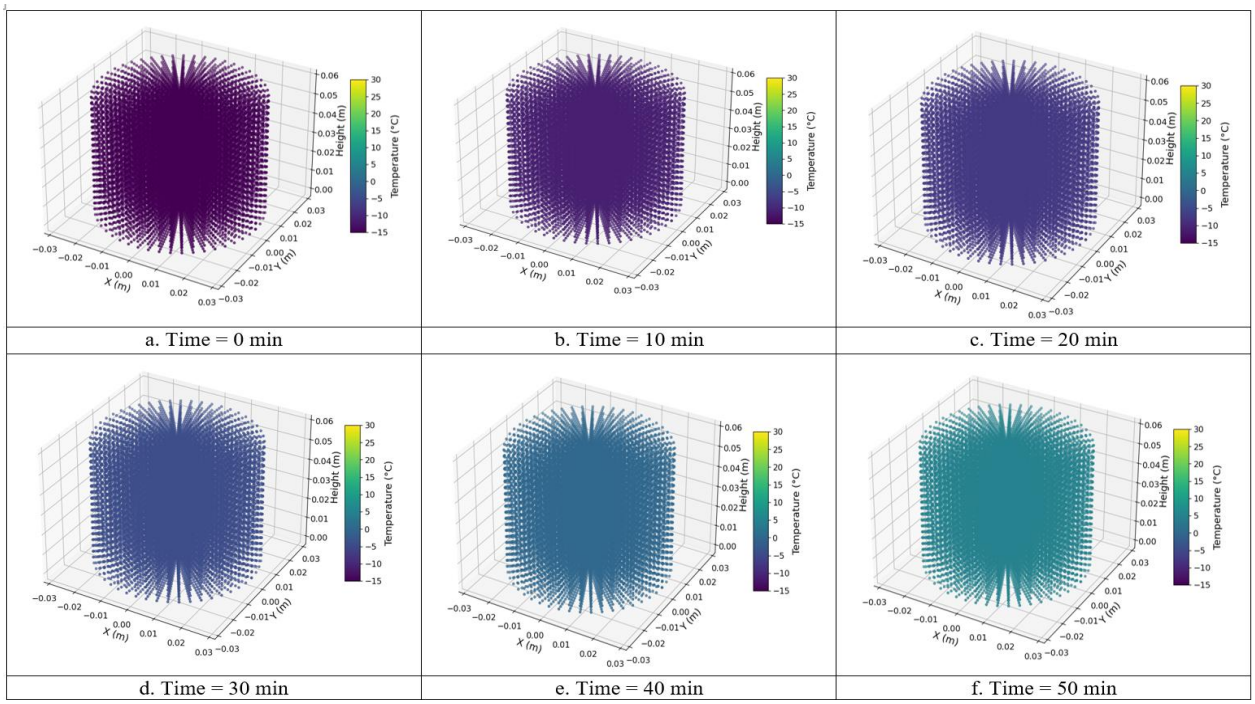


Figure: 4 Experimental setup based on in-direct radiative convective environment



a. Time = 0 min	b. Time = 10 min	c. Time = 20 min
d. Time = 30 min	e. Time = 40 min	f. Time = 50 min

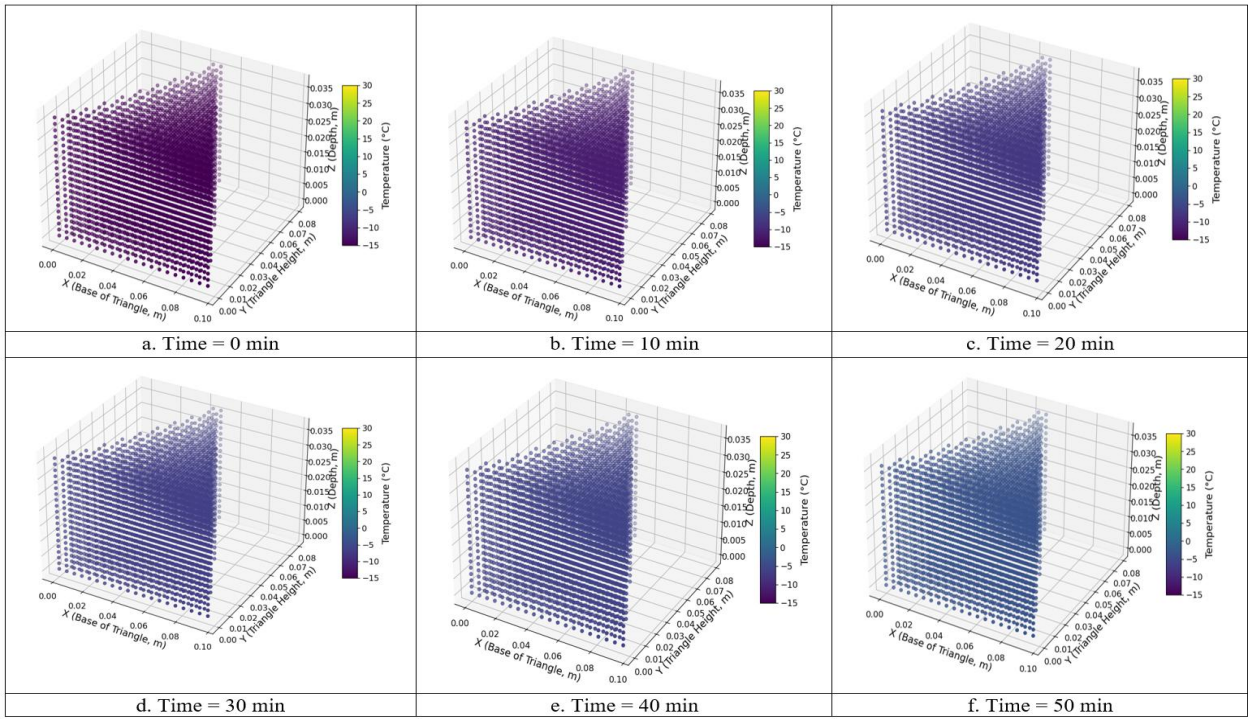
Fig 5: Simulation of temperature points in rectangular geometry considering uniform temperature distribution



a. Time = 0 min | b. Time = 10 min | c. Time = 20 min

d. Time = 30 min | e. Time = 40 min | f. Time = 50 min

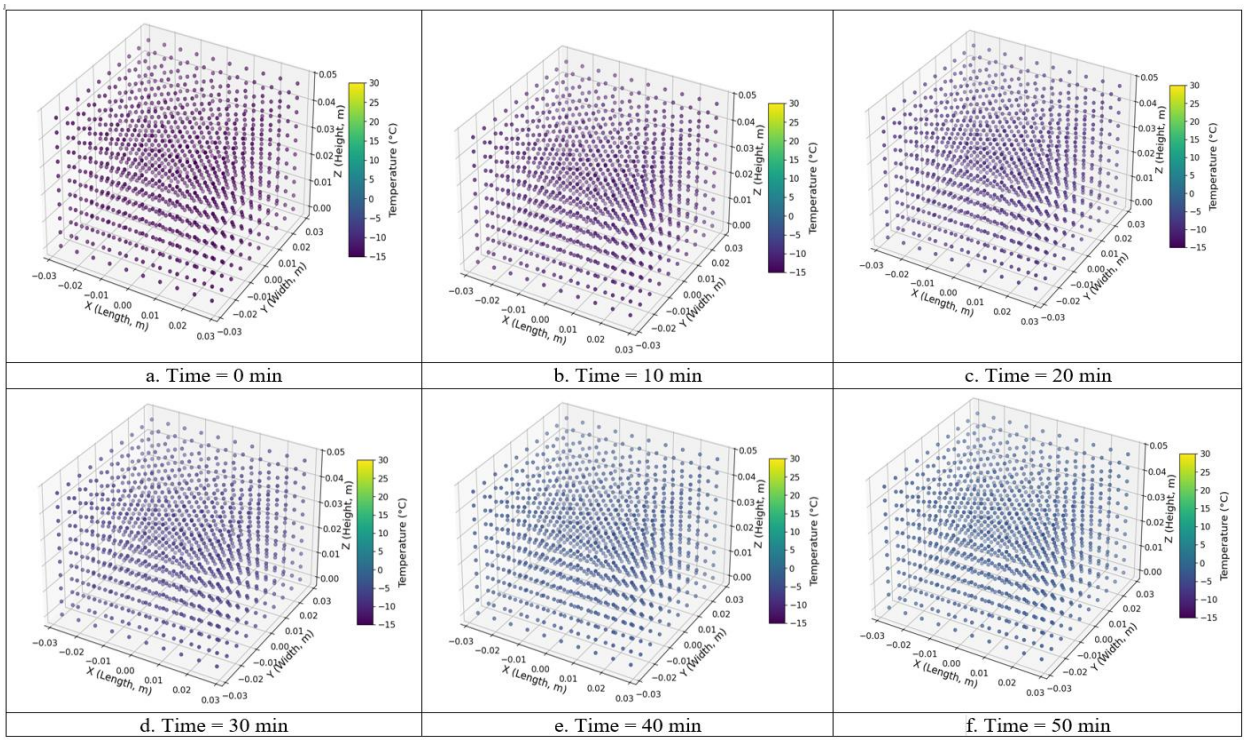
Fig 6: Simulation of temperature points in cylindrical geometry considering uniform temperature distribution



a. Time = 0 min | b. Time = 10 min | c. Time = 20 min

d. Time = 30 min | e. Time = 40 min | f. Time = 50 min

Fig 7: Simulation of temperature points in triangular geometry considering uniform temperature distribution



a. Time = 0 min | b. Time = 10 min | c. Time = 20 min

d. Time = 30 min | e. Time = 40 min | f. Time = 50 min

Fig 8: Simulation of temperature points in square geometry considering uniform temperature distribution

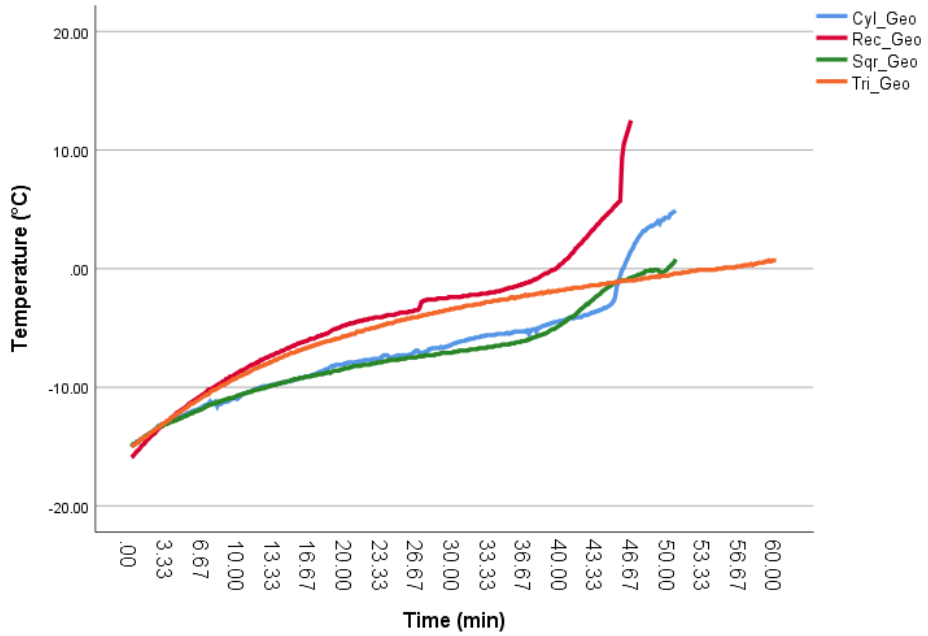


Figure 9: Temperature profile (melting) of PCM in different geometries

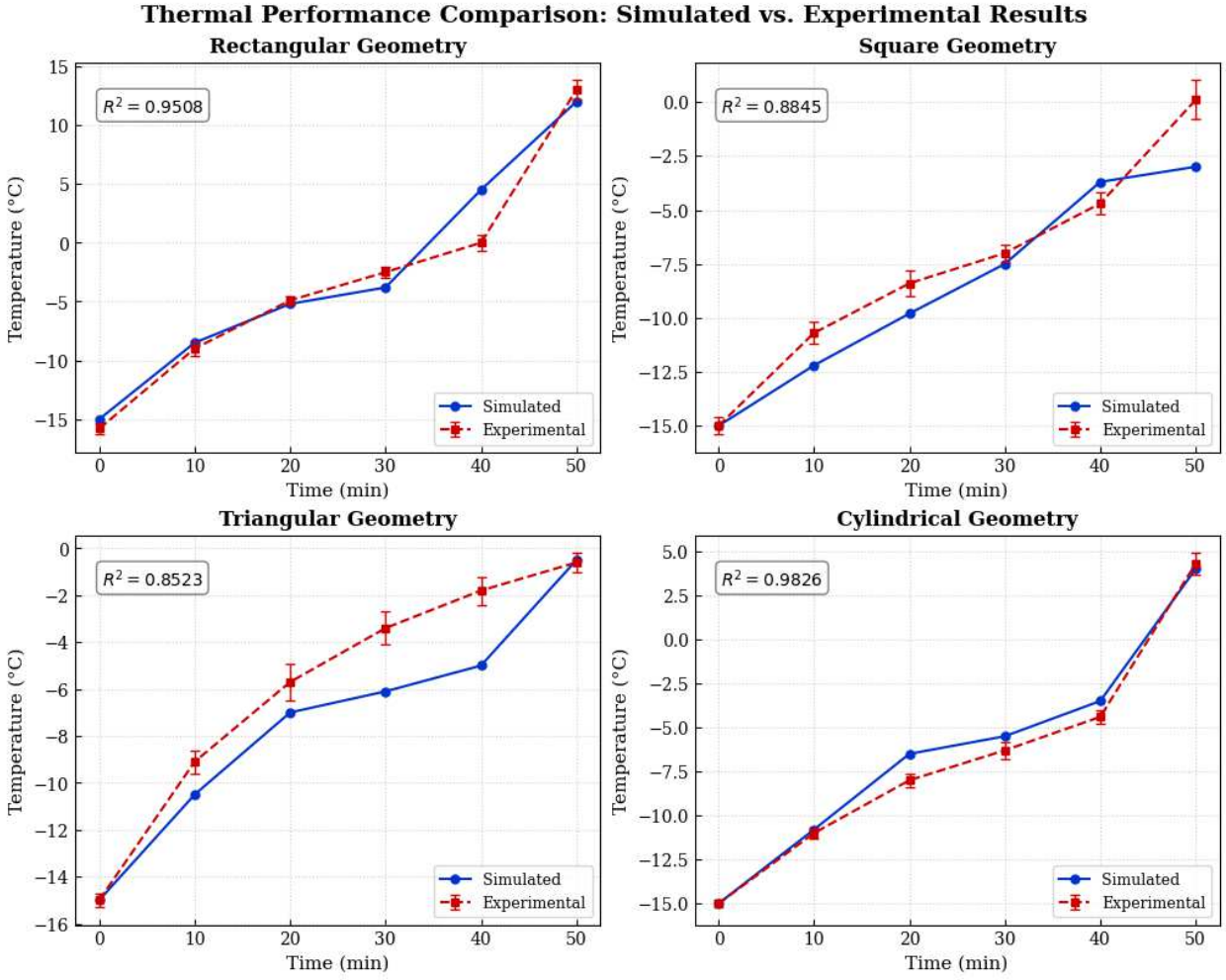


Figure 10: Comparison of Simulated vs experimental temperature profile at specific time interval

Supplementary Files

This is a list of supplementary files associated with this preprint. Click to download.

- graphicalabstract.jpg